Exploring the Relationship Between Depth and Light Intensity at Different Frequencies

James P. Fernandez[1], Caleb H. Norfleet[1], and Daniel J.M. Rohde[1], *Team 5, Section 2, May 8th, 2019*

***Abstract*— This paper presents the design of and experiments conducted using an autonomous underwater vehicle for the final project of Harvey Mudd College's Experimental Engineering course. The vehicle was outfitted with sensors to measure pressure, tubidity, and light intensity with the ultimate goal of assessing the viability of using light intensity to measure depth. This vehicle was deployed at three separate sites during the process of this experiment: the Bernard Field Station, Pitzer College's swimming pool, and Dana Point. While the team determined that noise in light intensity measurements made implementation of live depth-finding using light difficult, post processing the data using a moving average function allowed the team to construct a fit between voltage versus depth in the expected exponential form. In the IR light range used, the relationship was $V(z) = Ae^{Bz}$ where $A = 158.4 \pm 6.15$ and $B = -0.03227 \pm 0.0024$ (95% confidence). This fit had $R^2 = 0.923$. It was concluded that using light as a means of depth-finding is feasible, but would require more noise reduction equipment due to the post processing required to obtain this result as well as the team's inability to achieve similar success on other calibration runs.**

I. Introduction

The goal of this project was to explore the potential of using the absorbance spectrum of light by water to determine the depth of an autonomous underwater vehicle (AUV) as an alternative to using a pressure sensor. An AUV was constructed to collect data on pressure, turbidity, and light levels at two different frequencies. This data would enable the creation of a calibration curve for converting the intensity of the sunlight detected at the two different frequency ranges to a calculated depth value.

$$I(z) = I_0 * e^{-z\alpha} \quad (1)$$

It was expected that as light penetrates a material, the intensity of the light will fall off at an exponential rate with penetration depth (1) due to the Beer-Lambert Law [1]. The rate at which the intensity falls off was known to be a function both of properties of the material and of the spectra of frequencies present in the light. It was also known that water absorbs light in the infrared (IR) range much more than in the visible light range (Figure 1).

Figure 1. Absorbance Spectra for Water [2] [3]

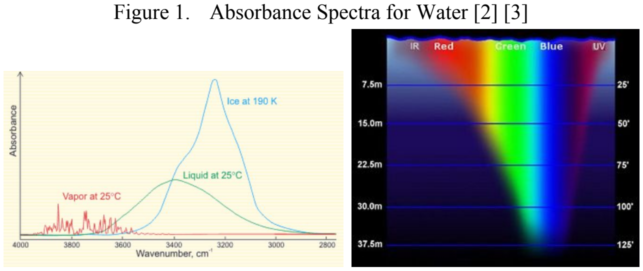

[1] All authors are with the Department of Engineering, Harvey Mudd College, Claremont, CA 91711

As a result of this difference in absorbance, it was concluded that IR light would fall off in intensity with a higher exponential rate than visible light. Thus, assuming that the ratio of IR and visible light in sunlight at the water surface is roughly constant independent of the time of day, weather, and other environmental factors, it was hypothesized that the ratio of the intensity of light at these spectra underwater will be purely a function of the depth underwater.

It was known that one factor which could impact the the absorbance spectra and thus our calibration curve was silt, microorganisms, and other material suspended in the water. As a result, it was desired to use a turbidity sensor to quantitatively explore how these factors might impact experimental results.

II. Experimental Setup

A. Engineering Goal

For this project, the team was interested in exploring the viability of using the intensity of light detected at a particular depth as an alternative to the standard pressure sensor. While light sensing was thought to be liable to vary greatly based on weather conditions, the team thought it would be worthwhile to explore the ease of setup and calibration, the accuracy, and the cost effectiveness of such a sensor when compared to a pressure sensor.

B. Sensor Selection

The team selected three distinct sensors to measure relevant quantities in their experiments. These sensors were a pressure sensor, a turbidity sensor, and visible light and infrared light photodiodes.

The MPX5700 pressure sensor was selected as a way to measure depth [4]. This sensor would have two main uses. The first would be to allow the autonomous navigation of the AUV frame while light intensity at depth data was collected in order to calibrate the photodiodes. The second would be to record the depth measured on a subsequent run while the AUV navigated depths using the photodiodes. These measurements would be used following the experiment to compare the readouts of the sensors and access the accuracy of the photodiode depth measurement

An 1R1503 IR LED and two OP950 IR photodiodes were used to construct a turbidity sensor [5,6]. The turbidity sensor was selected as an auxiliary sensor due to its relevance in the ultimate results of the experiment. Water with higher values of turbidity, a measurement of magnitude of external contaminants in the water, could impact the amount of light reaching the sensor, thus skewing depth measurements. This sensor was included as a way of potentially explaining strange results/behaviour of the AUV.

Figure 2. Current Output Characteristics of Photodiodes Used for IR (Left [7]) and Visible Light (Right [8]) Provided by Datasheets

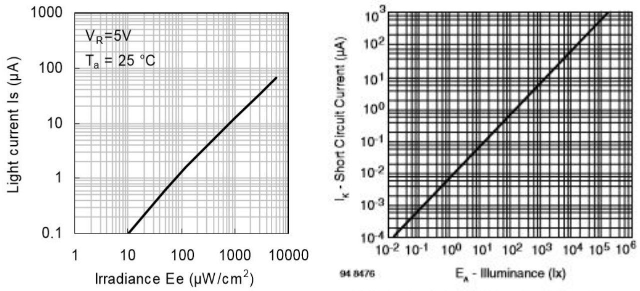

Figure 3. Wavelength Dependent Output Characteristics of Photodiodes Used for IR (Left [7]) and Visible Light (Right [8]) Provided by Datasheets

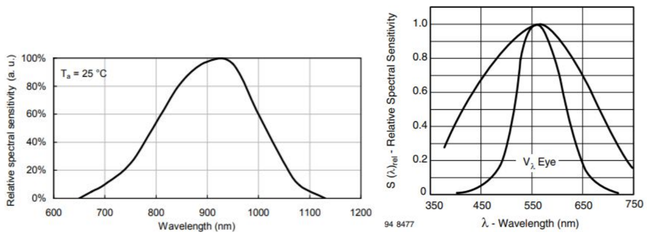

The WP3DPD1BT/BD IR photodiode and the BPW21R visible light photodiode were selected as a means of measuring the light intensity at depth [7,8]. Photodiodes are sensors that transmit a current based on the intensity of the light that reaches the sensor. These two particular photodiodes were selected for use in this project due to their frequency response spectrum and linear relationship to intensity changes. As shown in Figure 2 above, both sensors respond linearly to intensity over several decades of response. As previously discussed in the introduction, water has different absorption of light based on the depth [2,3]. IR light is absorbed early on, while green and blue light go deeper into the water before being absorbed (see Figure 1). Thus, these two particular IR and visible light photodiodes were chosen due to their sensitivity to the frequency spectrum of interest, shown above in Figure 3.

C. Pressure Sensor Circuit Design

In order to determine the depth of the robot, a MPX5700 pressure sensor was used. From the pressure sensor datasheet, it was found that a voltage output range from 0.2 V to 0.7 V was expected from the surface (sea level) to a depth of 8 meters [4]. As a result, a 6.2x gain op-amp circuit with an offset of -1.1 V was created to increase the resolution of our measurements (Figure 4) (2). The MCP601 op-amp [9] was supplied with 3.3 V to ensure that the output would be clipped at the maximum acceptable input voltage for the Teensy.

$$V_{out} \approx R_f\left(\frac{1}{R_1}+\frac{1}{R_2}+\frac{1}{R_f}\right)V_{pressure} - 5\frac{R_f}{R_1} \quad (2)$$

Figure 4. Pressure Sensor Circuit Schematic

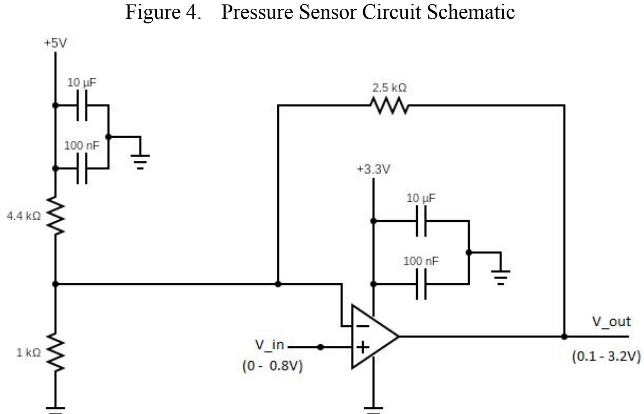

D. Turbidity Sensor Circuit Design

A turbidity sensor was constructed using an IR LED and two photodiodes placed directly across from and at a 90 degree angle from the LED (Figure 5). The turbidity sensor works by measuring the amount of light hitting each photodiode. When turbidity is high, more IR light is reflected by particles in the water so the ratio of the 90 degree photodiode voltage to the directly across photodiode voltage is larger. In order to reduce the impact of varying intensities of IR light in the background, a synchronous detection design was utilized in which the IR LED is flashed on and off approximately once per second. A mathematical filtering technique was used to isolate the amount of photodiode voltage change which is due to the IR LED from the voltage change due to background light.

Photodiodes act like current sources with a current output which is proportional to the intensity of IR light detected. Thus, in order to enable the Teensy to determine the amount of IR light detected, a transimpedance amplifier was created to convert the current output of the photodiode to a voltage output (Figure 6). It was experimentally determined that the photodiode had a maximum typical

Figure 5. Turbidity Sensor Design

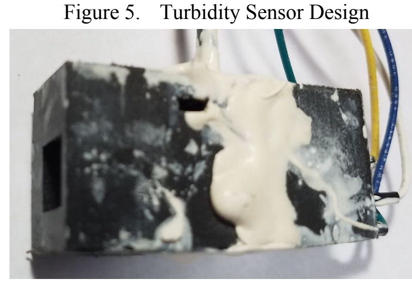

Figure 6. Turbidity Sensor Circuit Schematic

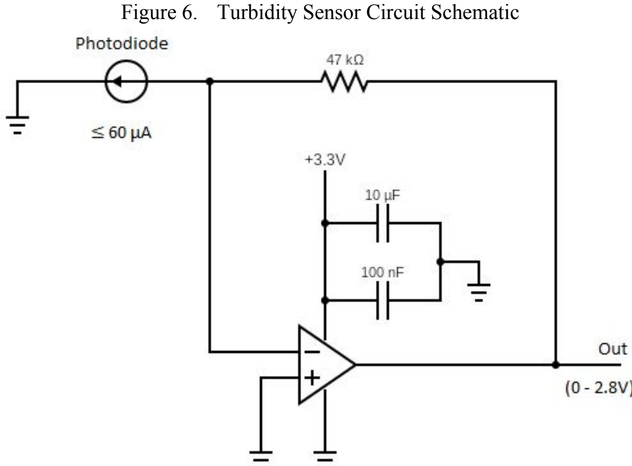

Figure 7. Square Wave Generation Circuit for Turbidity Sensor

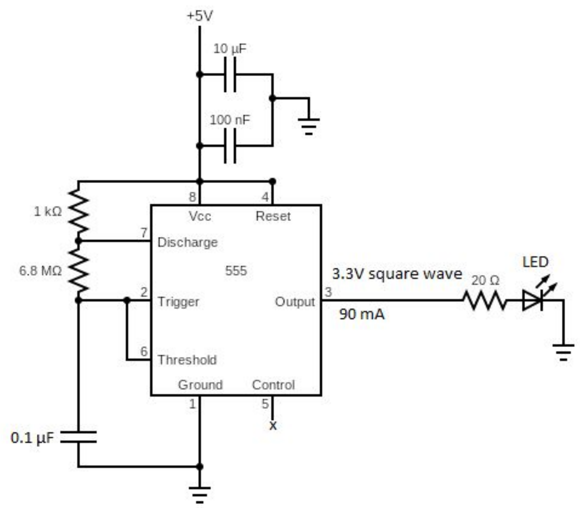

current value of 60 µA, so resistance values were selected to result in expected output voltages from 0 V to 2.8 V (3).

$$V_{out} \approx RI \quad (3)$$

In order to cause the IR LED to flash on and off and thus enable the use of a synchronous detection design, it was necessary to generate a square wave to power the LED. This goal was accomplished by using a 555 chip in astable oscillation mode (Figure 7) [10]. Resistance and capacitance values were selected for this circuit to result in a frequency of approximately 1.06 Hz (4). Since it was known that the sampling frequency of the Teensy was 10 Hz, this frequency was selected so as to be less than the Nyquist frequency of f_s / 2 = 5 Hz to avoid aliasing and folding [11].

$$frequency \approx \frac{1.44}{(R_A+2R_B)C} \quad (4)$$

E. *IR and Visible Light Sensor Circuit Design*

In order to measure light levels from sunlight in both IR and visible light ranges, a pair of photodiode circuits were used. Transimpedance amplifier circuits similar to those for the turbidity sensor were used to convert the current output

Figure 8. Light Sensor Circuit Schematic (Values Shown in Table 1)

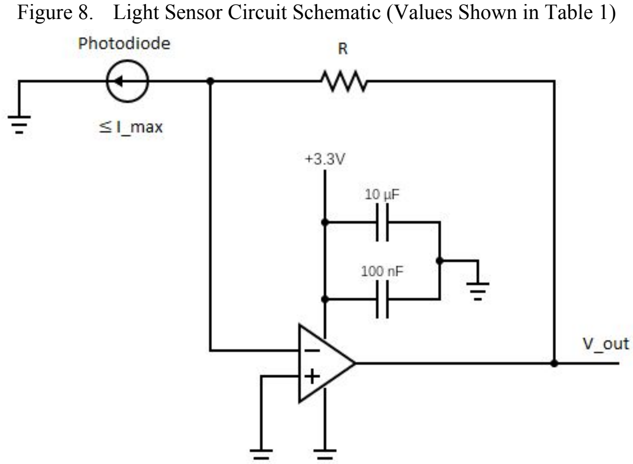

Table 1. Light Sensor Circuit Values

Light Type	IR	Visible
I_{Max}	145 µA	1070 µA
R	18 kΩ	2.4 kΩ
V_{out}	0 - 2.6 V	0 - 2.6 V

of the photodiode to a voltage output and thus enable the Teensy to measure the intensity of light in these ranges (Figure 8). It was determined experimentally that at noon on a sunny day the visible light photodiode output a maximum typical current of 1070 µA and the IR light photodiode output a maximum typical current of 145 µA. As a result, resistance values were selected to provide expected output voltages in the range from 0 V to 2.56 V for the visible light sensor and from 0 V to 2.61 V for the IR light sensor (3). These resistance values, the maximum expected current, and the sensor voltage swing are all summarized in Table 1.

F. *Sensor Modeling and Circuit Verification*

In order to verify the functionality of our sensors and also enable us to convert the voltage outputs read by the Teensy to relevant physical quantities, several calibration curves and expected sensor output models were created.

First, a calibration curve was created to convert the voltage output of the pressure sensor (in teensy units, where one teensy unit corresponds to 3.23 mV) to the depth of the top edge of the AUV in centimeters (Figure 9). It was found that the pressure sensor had relationship (5). Note that, as explained in Section III.A, it was necessary to later adjust this calibration curve to account for altitude differences (as it was created slightly above sea level).

$$depth = (1.5241 * voltage) - 210.13 \quad (5)$$

It was found that this calibration curve had a linear relationship, as expected, and that the R^2 value for the linear fit was very close to one (0.9994), as desired. This result gave a strong indication that the pressure sensor circuit was functioning properly. In order to further verify the functionality of the pressure sensor, a series of tests were done in which the AUV was placed at arbitrarily selected

Figure 9. Pressure Sensor Calibration Curve

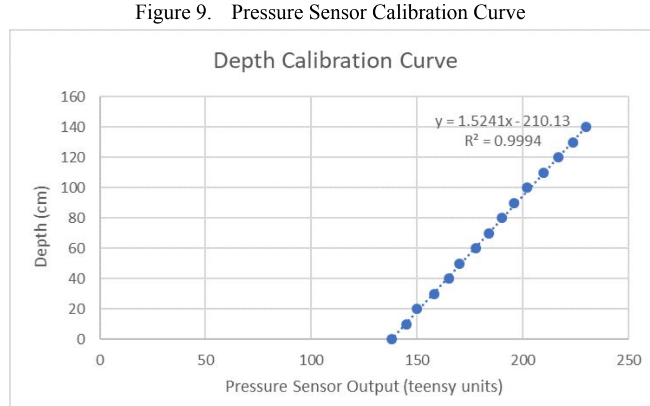

Figure 10. Turbidity Sensor Calibration Curve

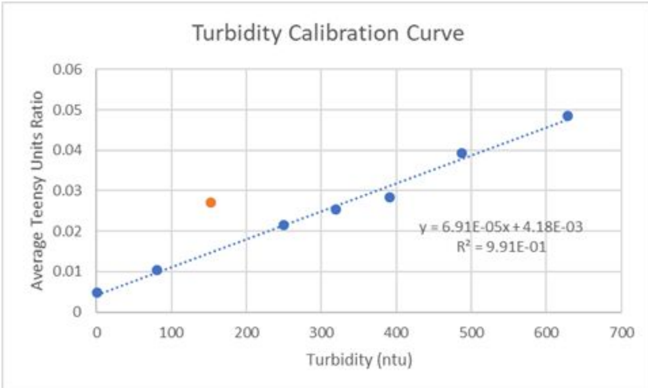

depths between zero and 1.5 meters, the Teensy calculated its depth using these calibration curve values, and then the actual depth was measured and compared to the calculated value. Over a dozen tests the Teensy consistently gave values within approximately three centimeters of the measured depth, so the pressure sensor was deemed to be operating successfully.

Next, a similar calibration curve (Figure 10) was created to convert the ratio between the voltage outputs of the 90 degree and 180 degree turbidity photodiodes to a turbidity measurement in nephelometric turbidity units (ntu). In order to calculate the ratio of the voltage outputs in a manner which would be independent of ambient IR light levels, a MATLAB script was created to use a synchronous-detection based design to filter out background levels of IR light. Using this MATLAB script, it was found that the turbidity sensor had relationship (6). Note that one of the calibration curve data points (shown as orange in Figure 10) significantly deviated from all other points, and was thus not included in the calibration curve.

$$turbidity = 14,471.78 * voltageRatio - 60.49 \quad (6)$$

The calibration curve had a linear relationship, as expected, and the R^2 value for the linear fit was very close to one (0.991), as desired. This result gave a strong indication that the turbidity sensor was functioning properly.

Finally, expected models were created for the light level sensors for ambient visible and IR light. The photodiodes used in the AUV to detect light respond linearly to light intensity, and the voltage output of the transimpedance amplifiers (discussed above in the circuit setup) are approximately equal to the current times the resistance of the circuit. As the Lambert-Beer law [1] states that light intensity in a material will fall off following an exponential decay, it was expected that the voltage would match closely to (7), where R is the resistance in the circuit, k is some proportionality constant between the photodiode current and intensity, I_0 is the intensity of light just below the surface of the water, α is an attenuation constant [1], and z is the depth under the surface.

$$V_{photodiode} \approx RkI_0e^{-z\alpha} \quad (7)$$

Figure 11. A Light Intensity Calibration Curve Model Test Using Generated Data with Arbitrarily Selected Exponential Coefficients

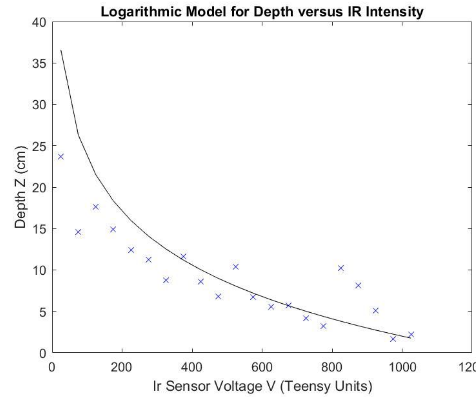

As can be seen in (7), a fit between voltage and depth (see Section III.D for why IR intensity was used directly instead of a ratio between IR and visible light intensities) can be done using only two constants, one representing the multiplicative factors and the other as the the optical depth constant in the exponent. This same relationship would also hold true for a voltage ratio, with the previously discussed constants now representing the combined physical parameters of the sensors and the light measured. A MATLAB script was created so that a calibration curve could be created and these two constants could be calculated once data was collected in field tests (Figure 11). MATLAB's "fit" function was used to perform a nonlinear, exponential fit on the voltage versus depth data, and these coefficients were used to solve for the coefficients in the depth versus voltage natural logarithmic fit. This software design was chosen due to the ease of implementation, as an exponential fit is built into the fit function and could easily be converted to logarithmic fit parameters.

G. *Mechanical Design*

The selected AUV design was a diving robot which would move autonomously and use P-control to travel to different desired depths. It was designed to travel to selected GPS location waypoints of interest on the surface and then dive down, stopping at different selected depths to take take measurements of light levels and turbidity and log the data. It would then return to the surface and head back to be shore to be collected.

As shown in Figure 11, a tall rectangular prism shape was selected for the AUV in order to maximize the distance between the motors and the IMU (and thus reduce interference with the magnetometer) while maintaining a low profile against currents (and wind). The two light sensors were placed at the top edge of the AUV facing upwards to maximize light exposure, and the turbidity sensor and pressure sensor are placed at the top edge of the other side of the frame in order to take measurements at the same depth. The waterproof box is located right next to the sensors at the top and contains all the main electronics, including a Teensy Arduino microcontroller, and IMU, and a

Figure 12. Isometric View of AUV Mechanical Design

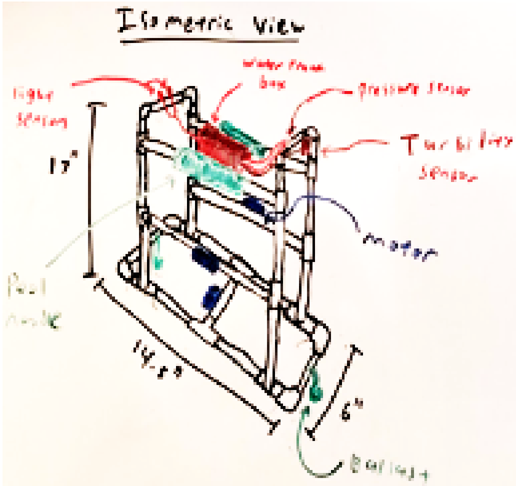

GPS. Three motors are located near the base of the AUV for navigation and diving.

The AUV was designed to be overall neutrally buoyant, making it easy to generate enough thrust to submerge and return to the surface. It was found that the robot has a total mass of 2.55 kg. In addition, it was calculated that the waterproof box and the pool noodles had buoyancy forces of 14.1 N and 6.82 N, respectively, so it was estimated that the total buoyant force on the AUV was 25 N. Thus, two ballasts each with a mass of 0.54 kg were be added to the AUV. Upon testing in a freshwater tank, it was found that the AUV was slightly positively buoyant, so 0.5 kg of additional ballast was added to make it as close to neutrally buoyant as possible (erring on the side of positive buoyancy as it was known that buoyancy would decrease slightly with depth due to pressure compressing the pool noodles). The ballast was further increased (by approximately 100 grams) for the Dana Point deployment to account for the difference in density between saltwater and freshwater.

Using symmetry, it was known that the center of pressure and center of mass would be located along the center z-axis

Figure 13. Front View of AUV Mechanical Design

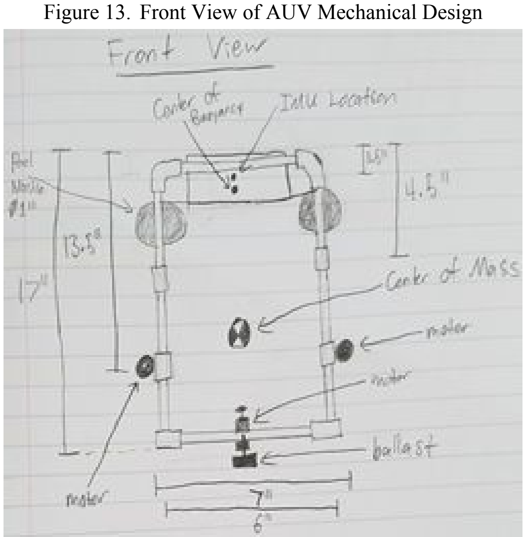

Figure 14. Final AUV Design

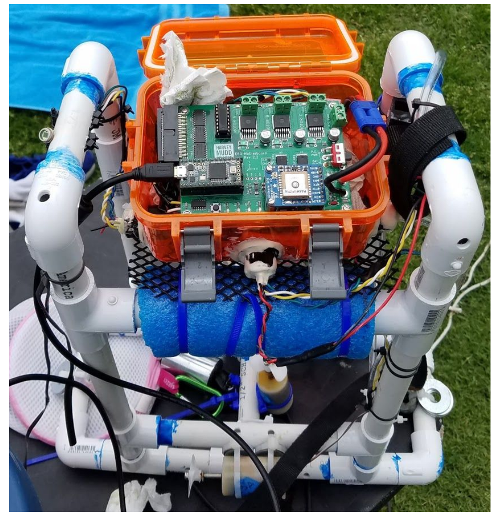

of the robot. It was calculated that the center of pressure was located 3” ± 0.5” from the top of the AUV and the center of mass was located 12.5” ± 0.5” from the top (Figure 13). Thus, since the center of pressure was significantly higher than the center of mass it was determined that the AUV will not flip over, as desired. The completed construction of the AUV is shown in Figure 14.

H. Experimental Procedure

Deployments were done close to noon in order to maximize sunlight brightness. For each deployment, the AUV was first connected to a laptop using a USB cable. Using the Arduino serial window, the robot’s GPS location was determined and used to set the desired GPS origin point in the robot code. In addition, desired waypoints were entered for the AUV. These waypoints would be travelled to in order and could consist of either travelling to a certain horizontal location or diving to a specific depth (and then waiting at that waypoint for a specified time interval, if desired). In general, the AUV’s path would consist of moving out from shore to a specific point, diving straight down, moving straight back to the surface, waiting for the GPS to re-connect to satellites, and then returning to shore.

Initially, it was planned that test runs would be conducted in which the AUV’s P-control diving system used both the pressure sensor and the light sensors in order to dive. However, after collecting data it was determined that the light sensors produced a signal that was too noisy for this approach to be successful, so all test runs were conducted using pressure-sensor-based P-control code for diving.

For each test run, after setting the GPS origin and waypoints, the code was redeployed to the Arduino, the microSD card was placed in the waterproof box, the Arduino was restarted, and then the waterproof box was closed and sealed. Next, after the GPS sensor connected to satellites (indicated by the side motors beginning to move), the motor behavior was examined to make sure the AUV was attempting to move in generally the correct direction and then the AUV was placed in the water and deployed.

After the AUV returned close to shore/the dock, it was collected and removed from the water. The frame was drained and excess water was removed with a towel. The microSD card was removed and data was downloaded to the laptop and analyzed using MATLAB.

III. Results and Analysis

A. Deployments Overview

In order to collect experimental data, the AUV was deployed at three different locations. First, the AUV was deployed in pHake lake at the Bernard Field Station (BFS) in Claremont, California. Unfortunately, it was highly cloudy and rainy of the day of the BFS deployment, which prevented the collection of usable light level data, but turbidity data was collected and valuable debugging experience was gained. It was discovered that the AUV had great difficulty reaching waypoints and would often circle around them instead of heading in the correct direction. This issue was determined to be a result of incorrect hard iron and soft iron coefficients for the magnetometer used to determine the orientation of the robot, so the magnetometer was re-calibrated, fixing the problem.

Next, the AUV was deployed in a swimming pool at Pitzer College in Claremont, California (Figure 15). Several successful tests were conducted, and the robot proved capable of navigating and diving autonomously and collecting data. After analyzing this data, it was noted that the light sensor data was much more noisy than anticipated (discussed further in section III.D). As a result, it was decided that it would be more successful to just use one of the two light sensors to create a depth calibration curve instead of using a ratio of the two sensor values (which would have magnified the noise significantly).

Finally, the AUV was deployed from beach and dock locations at Dana Point in California (Figure 16). For this location it was necessary to adjust the intercept of the pressure sensor calibration curve to account for a difference in altitude relative to other deployments. In addition, the ballasting used was slightly increased to account for the increased density of saltwater over freshwater (see section II.G). After these minor modification, the AUV was deployed and collected data successfully (even though it was cloudy for most of the day).

Figure 15. Deployment at Pitzer Pool

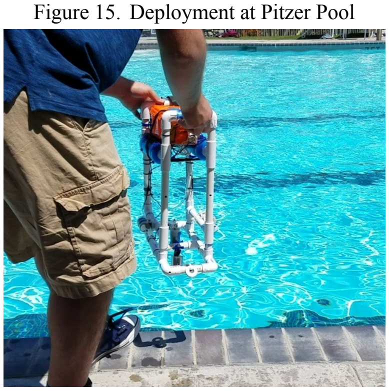

Figure 16. E80 Team with AUV at Dana Point

B. Pressure Sensor and P-Control Results

The pressure sensor proved to be a very consistent and accurate sensor for determining depth (±3 cm, see section II.F for validation and analysis). Although the GPS module was not able to determine horizontal position nearly as accurately (a standard deviation of 3-5 meters in position reading was observed when the module was stationary on dry land with more than six satellites connected), the combination of these two sensors enabled the successful creation of a proportionate control algorithm for navigating to desired waypoints and diving to desired depths.

In order to validate the operation of this code, tests were

Figure 17. Three Dives in Two Locations at Pitzer Pool. Horizontal Dashed Lines Indicate Depth Waypoints for Diving.

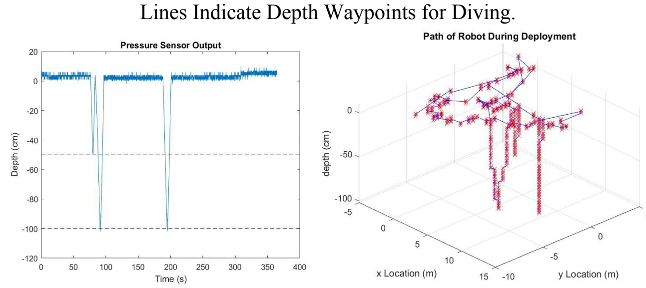

Figure 18. Diving and Hovering at Three Depths at Dana Point from Beach. Horizontal Dashed Lines Indicate Depth Waypoints for Diving.

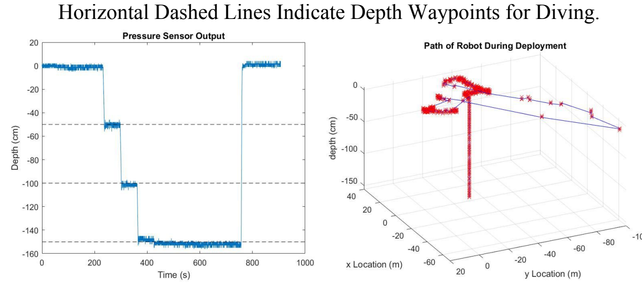

conducted in which the AUV navigated to different waypoints on the surface and then dove to selected depths. The AUV was successfully tested both for diving to specific depths and immediately resurfacing (Figure 17) and for maintaining selected depths stably for a specified amount of time (Figure 18).

C. Turbidity Sensor Results

Data on turbidity levels was also collected by the AUV. After data was collected, it was noticed that the turbidity values calculated based on sensor readings were significantly higher and more variable than had been anticipated. The data was further examined and it was discovered that this result appeared to be due to the impact of significantly higher background levels of IR light outdoors (due to sunlight) than had been present when testing the sensor in the lab.

Part of this impact was due to the fact that the op-amp circuit for the 180 degree photodiode was sometimes railing out due to the high background IR light levels. Excluding portions of the data in which this railing out occured (when the voltage measured by the Teensy was equal to 3.3 V) resulted in much more reasonable turbidity values.

The relative turbidites of the three deployment locations (Table 2) matched qualitative observations (Figure 19). However, it was noted that the average measured turbidity values still appeared to be surprisingly high relative to qualitative observations and expectations (Figure 20). Although the use of a synchronous detection algorithm for turbidity calculation should have hypothetically removed the impact of background IR light levels, it was hypothesized that it might still be affecting the data.

As a result, since it was known that IR light levels due to the sunlight would be significantly diminished even at shallow depths underwater, turbidity was re-calculated using only data from when the AUV was at a depth of more than half a meter (Table 2). This analysis resulted in values that much more closely matched expectations and which still made sense relative to each other give qualitative observations of the deployment locations. However, it is difficult to assess the uncertainty on these new measurements due to the fact that it was found that background conditions would significantly impact calibration curve values.

Table 2. Turbidity Measurements

Location	**Average Measured Turbidity**	**Average Turbidity While Diving (>0.5 m)**
pHake Lake	2700 NTU	N/A
Pitzer Pool	519.1 NTU	70.5 NTU
Dana Point	753.0 NTU	417.9 NTU

Figure 19. Water at BFS [12], Pitzer Pool, and Dana Point (Left to Right)

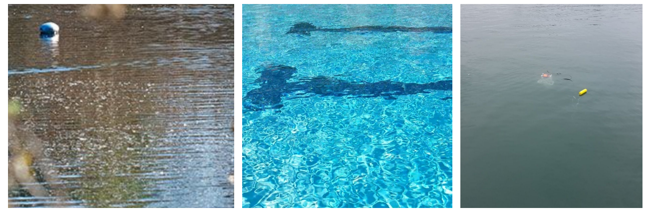

Figure 20. Solutions of Various Turbidites (Units in NTU) [13]

D. Light Sensor Results

The final set of sensor data that was collected was light intensity data in both IR and visible light ranges. Initially, it was hypothesized that it would be possible to use the ratio of IR light detected to visible light detected in order to make a depth calibration curve which would be independent of the light intensity at the surface. However, analysis of the data collected revealed much more variation in the signal than expected (Figure 21), and as a result it was concluded that the ratio of the two light signals would contain too much noise to be usable without more advanced filtering techniques. As a result, it was decided that depth calibration curves would be created just using the measured IR light level since it experienced a larger change in intensity per unit change in depth than the visible light level.

IR light level data was analyzed from a deployment at Pitzer College's pool at approximately 1:30 PM (Figure 22). Significant noise was observed in the signal, but this noise was significantly reduced when the AUV was underwater. It was hypothesized that this perceived noise was due to the

Figure 21. Light Level Data Collected During Test at Pitzer Pool

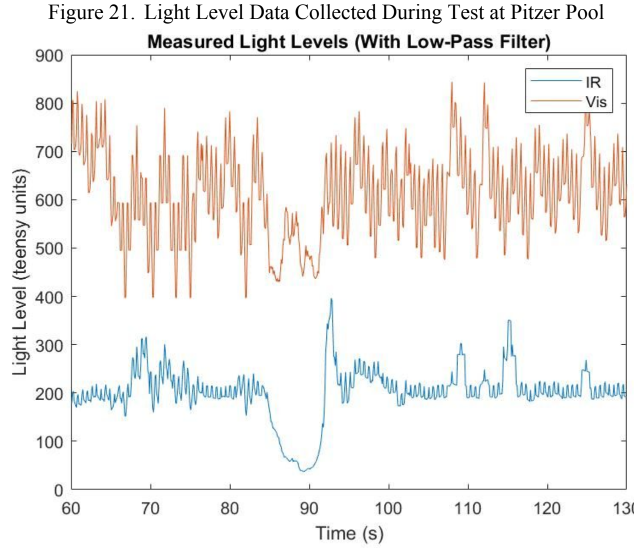

Figure 22. IR Light Depth Data from Test at Pitzer Pool

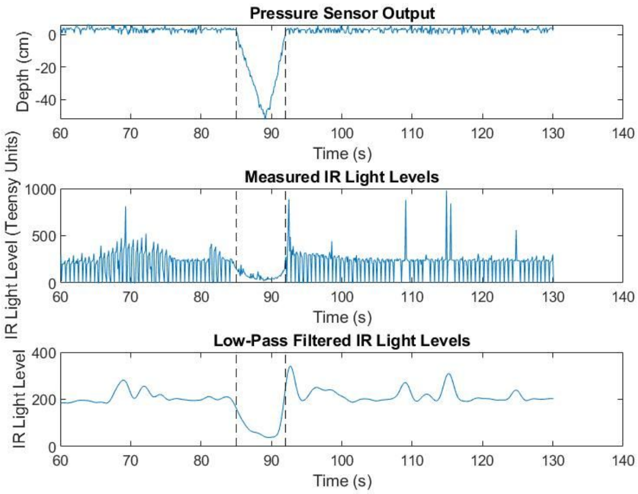

Figure 23. IR Light Depth Calibration Curve from Test at Pitzer Pool

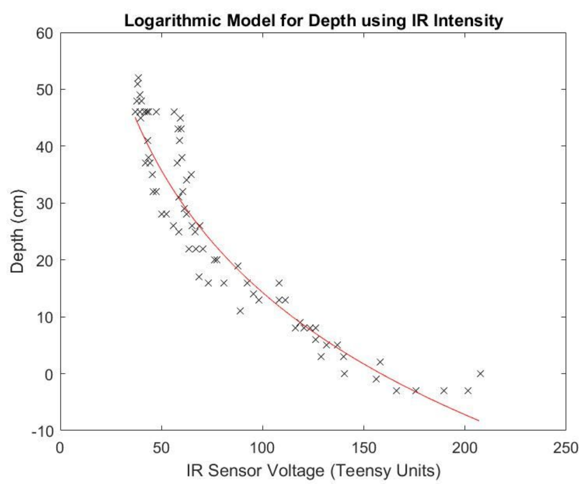

light sensor on the top edge of the AUV bobbing above and below the surface of the water, resulting in sudden changes in light incident on the sensor due to the fact that light would be reflected and scattered upon hitting the surface of water. Using just the segment of the data during which the AUV was diving underwater (indicated by vertical dashed lines in Figure 22), a calibration curve was created between depth and IR light intensity (Figure 23). Note that a logarithmic fit model was used due to the expectation that light intensity decays exponentially with depth. It was found that the measured voltage (in teensy units) from the IR sensor circuit and and depth (in cm) had relationship (8). The multiplicative coefficient had 95% confidence bounds (-33.288, -28.698) and the coefficient within the logarithm had 95% confidence bounds (0.00616, 0.00654), and the overall fit had an R^2 value of 0.923.

$$depth = -30.99 \ln(0.0063 * voltage) \quad (8)$$

IR light intensity data was also analyzed from a deployment from the dock at Dana Point at approximately 11:45 AM (Figure 24). Significantly more noise was observed in the signal from this deployment than the Pitzer

Figure 24. IR Light Depth Data from Dana Point Dock Deployment

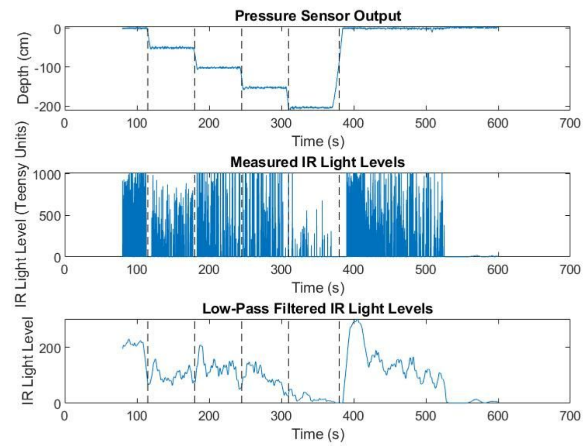

Figure 25. IR Light Depth Calibration Curve from Test at Dana Point

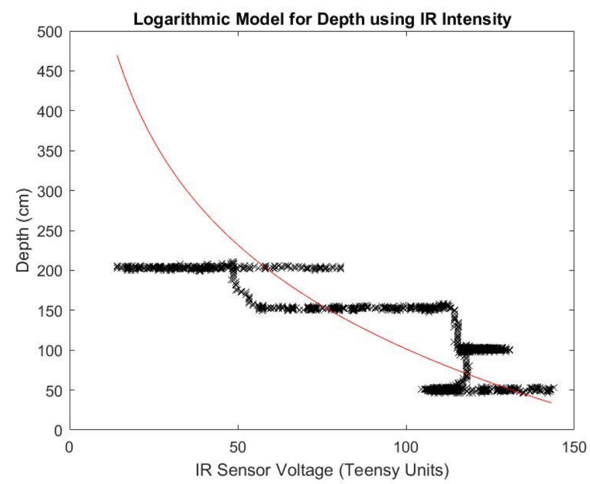

pool deployment, even when the AUV was underwater, made to rest stably at the same depth for a long time span, and with a low-pass filter applied to the dataset. As a result, the calibration curve which was generated using this data (Figure 25) is not a very good fit with an R^2 value of 0.639. It was found that the measured voltage (in teensy units) from the IR sensor circuit and and depth (in cm) had relationship (9). The multiplicative coefficient had 95% confidence bounds (-194.62, -181.93) and the coefficient within the logarithm had 95% confidence bounds (0.00578, 0.00591).

$$depth = -188.28 \ln(0.0058 * voltage) \quad (9)$$

It was hypothesized that this significant increase in noise which resulted in significant variation in measured voltage from the IR intensity sensor circuit at a constant depth was a result of the increase in wave activity at Dana Point compared to the deployment at Pitzer College's pool. It was known that when light penetrates the surface of water it will be refracted and reflected in a manner which is a function of the angle between the light and the surface of the water. When there are waves or ripples on the surface of the water, light intensity below the water's surface will thus vary

Figure 26. Typical Light Diffraction Pattern Underwater [14]

significantly with time and horizontal position, as can be seen in Figure 26.

After this data was collected and analyzed, it was compared to expected values found through initial research. The coefficient inside of the logarithm contains a parameter which represents the intensity of light immediately below the surface of the water, which would vary based on time of day and sunlight conditions. However, the multiplicative constant in front of the logarithm represents only parameters of the circuit, material properties of water, and the wavelengths of light being measured.

It was calculated that the coefficients from Figure 23 correspond to a light intensity decrease by a factor of 1/e for every every 31 centimeter increase in depth. That would correspond to a decrease in infrared light intensity of 96% at a depth of one meter relative to just beneath the surface. This result seems reasonable as it was known that red light diminishes significantly within a depth of less than five meters and IR light intensity falls off even more rapidly.

IV. Conclusion

A. Overall Results

While many overall goals of the project were not fully accomplished, the team achieved a number of successes in pursuit of larger goals.

The pressure sensor was throughout the project the most successful sensor used. In addition to being extremely well correlated to depth ($R^2 = 0.994$), this sensor also performed spectacularly as a means of navigation. In conjunction with the GPS navigation system, the pressure sensor was vital part of several successful autonomous data collection trips, working, including one case in which the vehicle navigated autonomously for nearly 10 minutes, much longer than the 1 minute requirement.

Despite overlooking the significance of background light in designing appropriate amplification for the turbidity sensor, the team was able to generate results that match qualitative comparisons between respective turbidity levels of the three deployment sites. In addition, the extremely correlated calibration curve the team created for the sensor ($R^2 = 0.991$) implies that slightly adjusting the amplification values to account for ambient light would have produced an extremely accurate sensor.

The light photodiodes, while the least successful sensors used, experienced enough success to justify further exploration of their use in depth-finding purposes. Despite ambient noise being too high for proper use in live depth finding or even adequately creating depth-intensity calibrations with post processing, the team managed to produce a single close relationship ($R^2 = 0.923$) among the two calibration curves discussed in Section III.D (shown in Figure 23). While such a result was difficult to obtain, it implies that further development could make this system more reliable, potentially to the point where it could see real-time use in autonomous navigation.

B. Significance of Results

In this project, the team worked to assess the effectiveness of using light as a means of depth-finding for an AUV. Though the results were mostly unsuccessful, there are promising signs if further work is done.

The importance of this work becomes clear when one considers both the economics of the situation and our search from the perspective of a designer. To purchase a single unit of the MPX5700 pressure sensor used in this project [4] costs $20.49. Purchasing one of the WP3DPD1BT/BD IR photodiodes [7] costs $0.99 (both prices from listings from Digikey Electronics [15]). Though the pressure sensor is significantly easier to work with, being more accurate, faster to calibrate, and having a linear relationship, figuring out a setup using the IR photodiode could contain a clear economic advantage.

From a design perspective, exploring new methods of accomplishing tasks traditionally done in a certain way is a worthy endeavor that can lead to new and interesting innovations. One should never limit their design space simply because a good choice already exists.

C. Recommendations for Future Work

As discussed in the light sensor results section (III.D), the team was in one instance able to accurately correlate the measured light intensity with the depth of the underwater. However, this only occured post-dive, and with serious cleanup off the data. Future look into light-based depth-finding would benefit from use of built-in noise-reduction mechanisms, including but not limited to analog filter circuits, use of multiple sensors with averaging, and built-in moving average code. The team believes these mechanisms could improve results to the point of being usable for live depth-finding navigation of the AUV.

Besides just using noise reduction mechanisms, the team also believes that work using non-IR photodiodes could provide positive benefits to the depth sensing. IR light penetrates less deeply that other types of light, so if such a photodiode could be made to work accurately, the maximum usage depth of the AUV diving in this manner could also be increased.

Acknowledgements

The team would like to acknowledge Erik Meike for helping us debug our motherboard when we accidentally shorted out the current sensor. We'd also like to thank all the E80 professors and lab proctors for making this semester a lot of fun!

References

[1] "Penetration Depth," *wikipedia.* Jan. 8 2019. [Online]. Available: https://en.wikipedia.org/wiki/Penetration_depth

[2] Chaplin, Martin. "Water Vibrational Spectrum". [online] Internet: http://www1.lsbu.ac.uk/water/water_vibrational_spectrum.html [Mar. 27, 2019].

[3] *Pix4d*. Diving Into Underwater Photogrammetry. [online] Internet: https://www.pix4d.com/blog/diving-into-underwater-photogrammetry [Mar. 27, 2019].

[4] NXP Semiconductors, "Integrated Silicon Pressure Sensor On-Chip Signal Conditioned, Temperature Compensated and Calibrated." MPX5700 Datasheet, Oct. 2012.

[5] Everlight, "5 mm Infrared Light, T-1 3/4" IR1503 datasheet, Oct. 2006.

[6] Jameco Electronics, "PIN Silicon Photodiode, Type OP950," Product Bulletin OP950, June 1996.

[7] Kingbright, "WP3DPD1BT/BD." WP3DPD1BT/BD datasheet. Aug. 3, 2018.

[8] Vishay Semiconductors, "BPW21R" BPW21R datasheet. Aug. 17, 2017.

[9] Microchip Technology Inc., "2.7V to 6.0V Single Supply CMOS Op Amp." MCP601 datasheet. Oct. 5, 2007.

[10] Fairchild Semiconductor Corporation, "LM555 Single Timer." LM555 datasheet. Jan, 2013.

[11] E80 Teaching Team. "Sampling, Aliasing, Folding." Internet: https://drive.google.com/file/d/1_lF1ZG382AHKLyA6_Bf0VBN1UHlD-eh_/view

[12] Hamlett, Nancy, "BFS contributes to the Great Backyard Bird Count." *research.pomona.edu*, Feb. 20, 2013. Available: https://research.pomona.edu/bfs/2013/02/20/bfs-contributes-to-great-backyard-bird-count/ [Accessed: May 5, 2019].

[13] J. Daly. Lecture Slides, Topic: "What is Turbidity." ISA NorCal, n.d.

[14] "Why does light at the bottom of a pool form this awesome pattern?" *physics.stackexchange*. Sept. 17, 2013. [Online]. Available: https://physics.stackexchange.com/questions/77586/why-does-the-light-at-the-bottom-of-the-pool-form-this-awesome-pattern [Accessed May 5, 2019].

[15] *Digikey Electronics*. [online] Internet: https://www.digikey.com/ [Mar. 27, 2019].

[16] E80 Teaching Team. "Reference AUV Turbidity Meter Procedure." Internet: https://docs.google.com/document/d/1RYaInz-txbC4iaJD83_0HSwKYBlVGDN1HlEs4yDEMjM/edit [Mar. 27, 2019].

[17] *Teensuduino 1.46*. PJRC Electronic Projects, 2019. Internet: https://www.pjrc.com/teensy/td_download.html [Mar. 27, 2019].

[18] Imboden, Connie. "The Science of Color Underwater". [online] Internet: http://connieimboden.com/2013/12/the-science-of-color-underwater-2.html [Mar. 27, 2019].

[19] *Frequencies of Light*. Frequently Asked Questions and Information. [online] Internet: https://www.frequenciesoflight33.com/16 [Mar. 27, 2019].

[20] "Sunlight" Internet: https://en.wikipedia.org/wiki/Sunlight [Mar. 27, 2019].

[21] B. Kuczenski, *hline and vline*. MathWorks File Exchange, 2001. Internet: https://www.mathworks.com/matlabcentral/fileexchange/1039-hline-and-vline [Mar. 27, 2019].

[22] Parashchenko, Oleg and Agilis IT Australia. *Online Syntax Highlighting for the Masses*. [online] Internet: https://tohtml.com/matlab/ [Mar. 13, 2019].

CODE APPENDIX 1: `processData.m` FUNCTION FOR ANALYZING DATA COLLECTED BY THE AUV

```
% Read in data
filenum = '003';
logreaderFunct

pressure = A15;
led      = A16;
turb180  = A00;
turb90   = A01;
vis      = A02;
ir       = A03;

% Convert data using calibration curves
t     = double(time) ./ 1000;     % in seconds
depth = A15 .* 1.524 - 210.13; %-55.84;    % in cm
NTU   = getTurb(turb180, turb90); % in NTU

% Plot path of AUV in 3D
figure(1)
plot3(x,y,-depth,"rx")
hold on
plot3(x,y,-depth,"b-")
hold off
title('Path of Robot During Deployment')
xlabel('x Location (m)')
ylabel('y Location (m)')
zlabel('depth (cm)')

% Plot depth of AUV
figure(2)
plot(t, -depth);
title("Pressure Sensor Output")
ylabel("Depth (cm)")
xlabel("Time (s)")

% Plot turbidity
figure(3)
plot(t,NTU)
title('Measured Turbidity Levels')
xlabel('Time (s)')
ylabel('Turbidity (NTU)')
NTU(isinf(NTU)) = nan;
mean(NTU, 'omitnan')

% Plot measured light intensity
figure(4)
movavgIR  = movmean(ir, 10);
movavgVis = movmean(vis,10);
plot(t, movavgIR)
hold on
plot(t, movavgVis)
hold off
title('Measured Light Levels')
xlabel('Time (s)')
ylabel('Light Level (teensy units)')
legend('IR', 'Vis')

%Plot turbidity sensor voltage outputs
figure(5)
title("Turbidity Sensor Outputs")

subplot(2,1,1)
plot(t, turb180);
title("Passing Light Readout")
ylabel("Voltage")
xlabel("Time")

subplot(2,1,2)
plot(t, turb90);
title("Reflected Light Readout")
ylabel("Voltage")
xlabel("Time")
```

CODE APPENDIX 2: `lightsensor_calibration.m` FUNCTION FOR CREATING A DEPTH CALIBRATION CURVE USING A LOGARITHMIC FIT MODEL OF IR LIGHT INTENSITY DATA

```
% Create x,y variables for the exponential model
x_exp = depth;
y_exp = V_ir;

% Create a fit for the data in the form V(z) = A*exp(B*z)
[exp_model, exp_gof] = fit(x_exp, y_exp, "exp1");
coeffs = coeffvalues(exp_model);

% Convert this model to the form z(V) = C*ln(D*V)
C = 1/coeffs(2);
D = 1/coeffs(1);
x_model = (min(x_log)):1:(max(x_log));
log_model = C*log(D*x_model);

% Plot our model
plot(x_log, y_log, "kx")
hold on;
plot(x_model, log_model, "r")
hold off;
title("Logarithmic Model for Depth using IR Intensity")
```

```
xlabel("IR Sensor Voltage (Teensy
   Units)")
ylabel("Depth (cm)")
```

CODE APPENDIX 3: `plottingIR.m` FUNCTION FOR CREATING PLOTS OF IR LIGHT INTENSITY DATA

```
s = 800;  % start of dive
e = 6000; % end of dive

line1 = 115;
line2 = 180;
line3 = 245;
line4 = 310;
line5 = 380;

ir2 = ir(s:e);
depth2 = depth(s:e);
t2 = t(s:e);
movavgIR2 = movavgIR(s:e);

figure(1)
subplot(3,1,1)
plot(t2, -depth2);
hold on;
vline(line1, 'k--');
vline(line2, 'k--');
vline(line3, 'k--');
vline(line4, 'k--');
vline(line5, 'k--');
hold off;
title("Pressure Sensor Output")
ylabel("Depth (cm)")
xlabel("Time (s)")

subplot(3,1,2)
plot(t2, ir2);
hold on;
vline(line1, 'k--');
vline(line2, 'k--');
vline(line3, 'k--');
vline(line4, 'k--');
vline(line5, 'k--');
hold off;
title('Measured IR Light Levels')
xlabel('Time (s)')
ylabel('IR Light Level (Teensy
   Units)')

lowpassir = lowpass(double(ir),
   0.01, 10);
lowpassir = movmean(
   lowpassir(s:e),100);
subplot(3,1,3)
plot(t2, lowpassir);
hold on;
vline(line1, 'k--');
vline(line2, 'k--');
vline(line3, 'k--');
vline(line4, 'k--');
vline(line5, 'k--');
hold off;
title('Low-Pass Filtered IR Light
   Levels')
xlabel('Time (s)')
ylabel('IR Light Level')
```

CODE APPENDIX 4: `getTurb.m` FUNCTION FOR CALCULATING TURBIDITY VALUES

```
function [NTU] =
   getTurb(turb180,turb90)

turbiditySlope     = 14471.780;
turbidityIntercept = -60.492;

signal180 = double(turb180);
signal90  = double(turb90);

avg180 = movmean(signal180,50);
avg90  = movmean(signal90,50);

signal180high = signal180;
signal180high(signal180high<avg180)
   =nan;
avgs180high = movmean(
   signal180high,50,'omitnan');

signal180low = signal180;
signal180low(signal180low>avg180)
   =nan;
avgs180low = movmean(
   signal180low,50,'omitnan');

signal90high = signal90;
signal90high(signal90high<avg90)
   =nan;
avgs90high = movmean(
   signal90high,50,'omitnan');

signal90low = signal90;
signal90low(signal90low>avg90)=nan;
avgs90low = movmean(
   signal90low,50,'omitnan');

rat = (avgs90high-avgs90low)
   ./(avgs180high-avgs180low);
%averageRat = mean(rat);
NTU = rat .* turbiditySlope +
   turbidityIntercept;

end
```